Electronic Supplementary Material (ESI) for Journal of Materials Chemistry A.

Supporting Information

Roles of self-reconstruction layer in catalytic stability of NiFeP catalyst during oxygen evolution reaction

Fuzhen Zhao[a], Xinyu Mao[a], Xin Zheng[b] Huicong Liu[a], Liqun Zhu[a], Weiping Li[a], Ze Wang[a], Haining Chen[a,*]

[a] *School of Materials Science and Engineering, Beihang University, No. 37 Xueyuan Road, Haidian District, Beijing 100191, China*

[b] *State Key Laboratory of Heavy Oil Processing, China University of Petroleum, Beijing 102249, China*

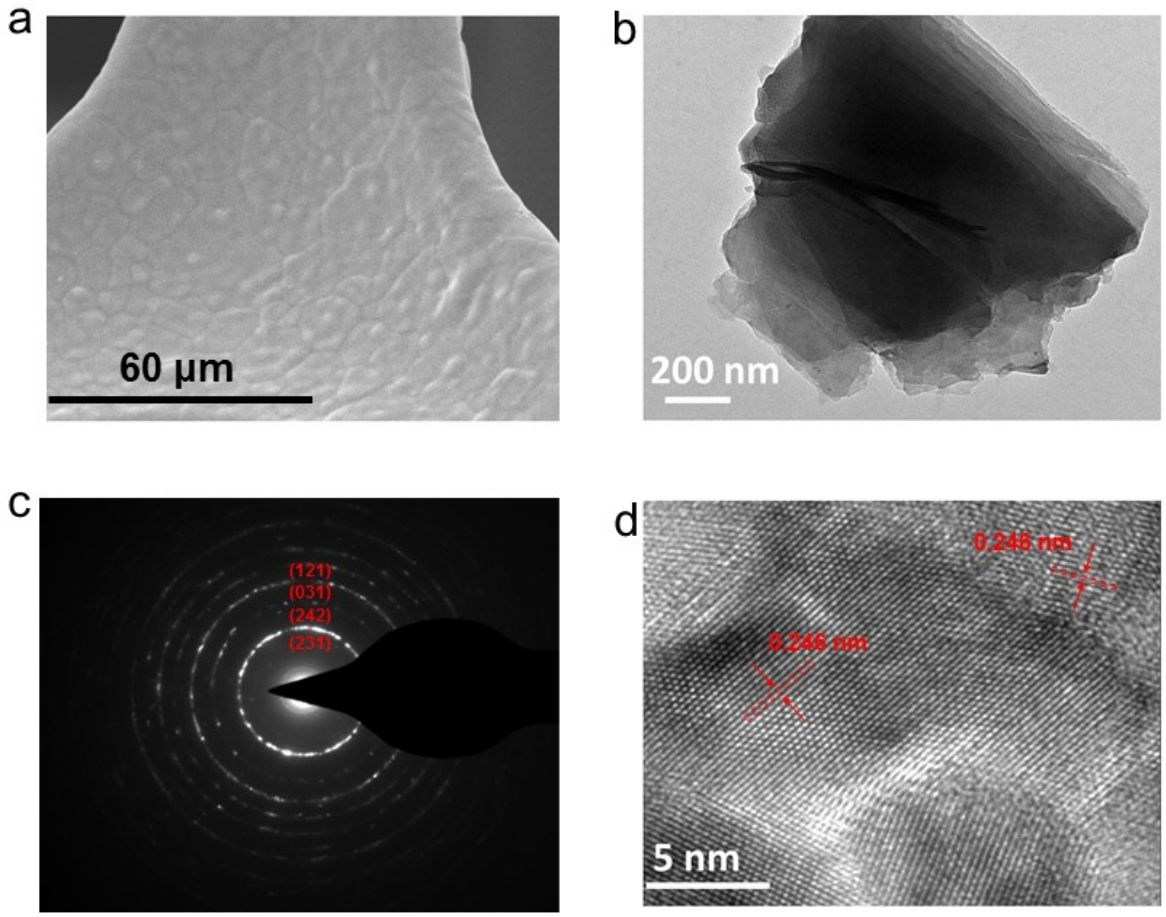

Figure S1. SEM and TEM Characterizations. (a) SEM image. (b) TEM image, (c) SAED pattern and (d) HRTEM image of polycrystalline $(Ni_{1-x}Fe_x)_3P$.

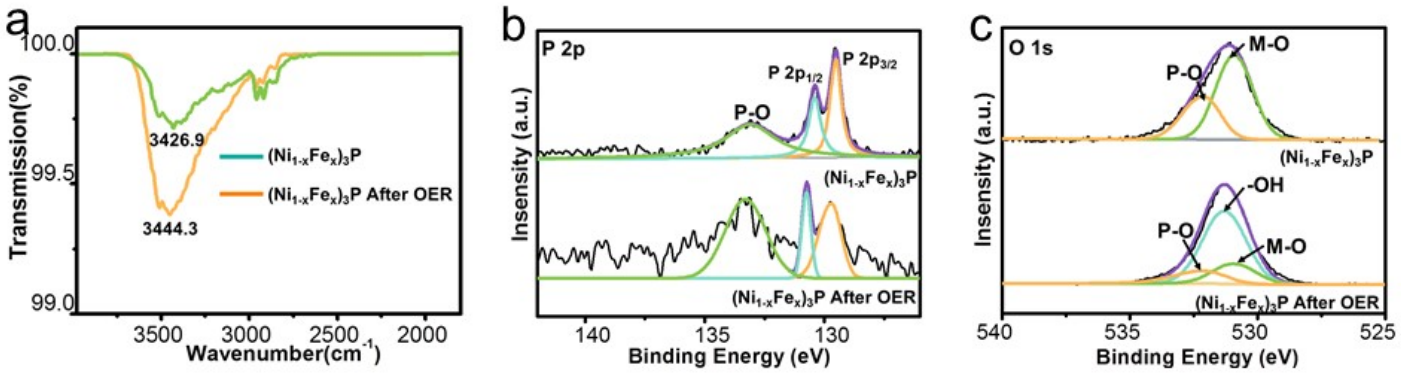

Figure S2. Characterizations of $(Ni_{1-x}Fe_x)_3P$ before and after stability measurement. (a) FTIR spectra. (b) P 2p XPS spectra and (c) O 1s XPS spectra.

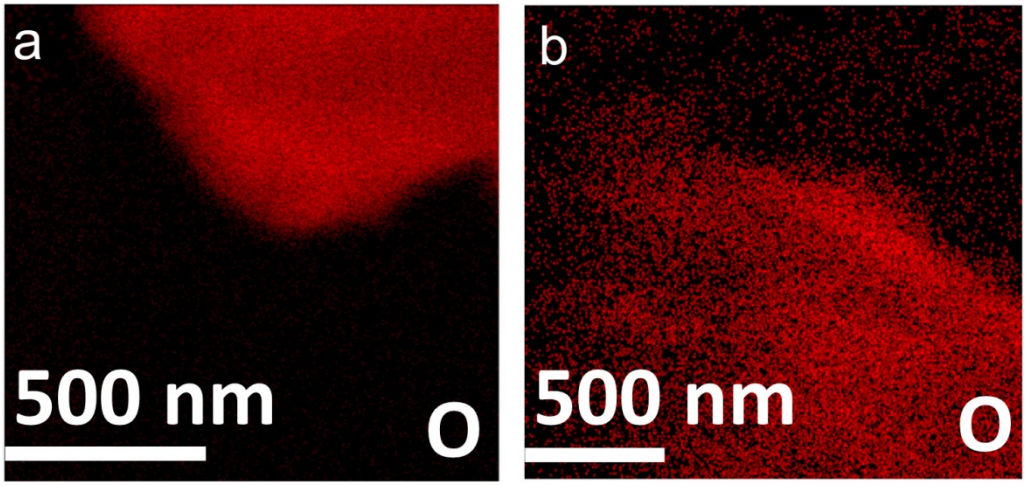

Figure S3. EDS mapping images of catalyst (a) before stability measurement and (b) after 30 h stability measurement.

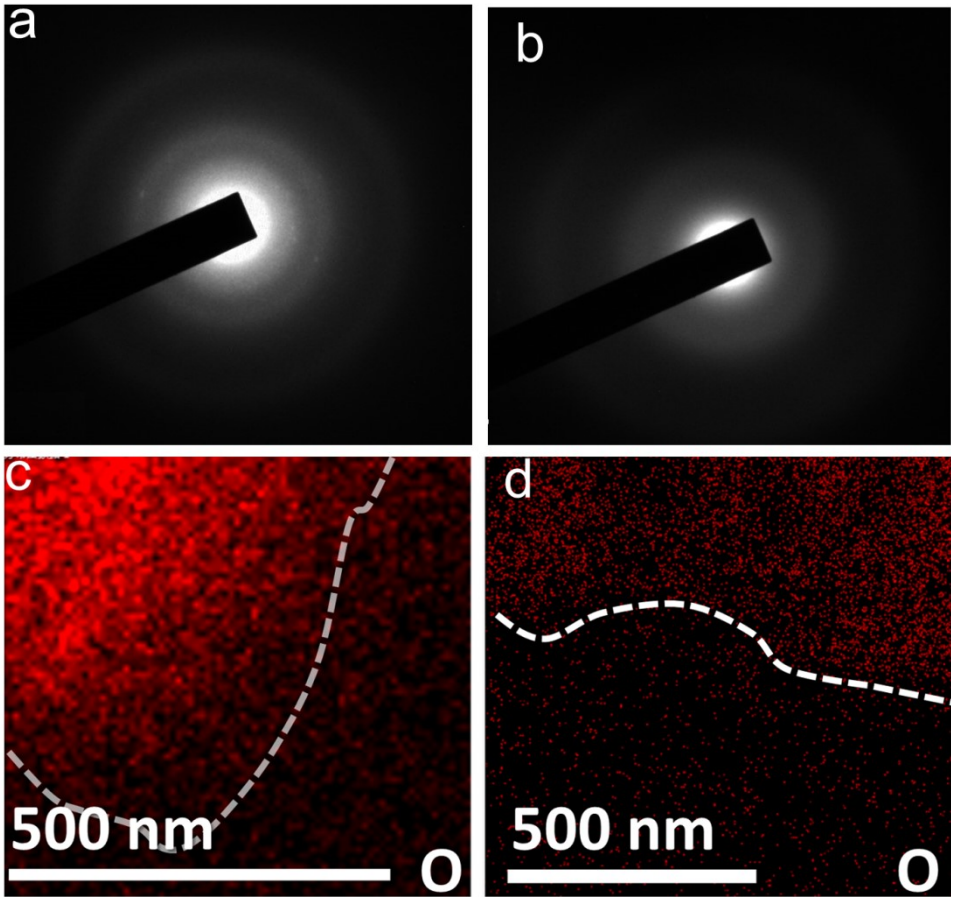

Figure S4. (a, b) SAED patterns and (c, d) EDS mapping images of exfoliated self-reconstruction layer (a, c) after 10 h stability measurement and (b, d) after 30 stability measurement.

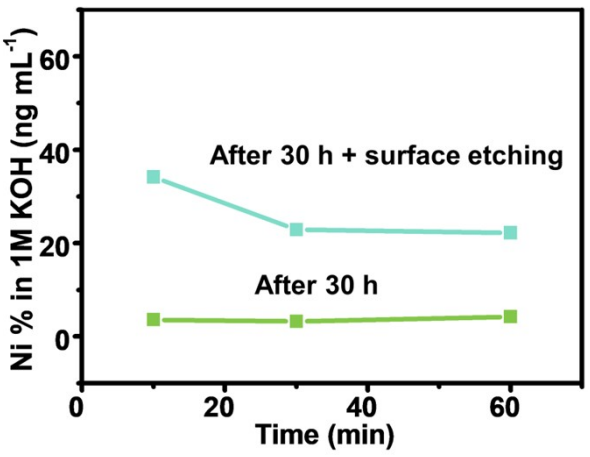

Figure S5. (a) Ni concentration in electrolyte at the current density of 100 mA cm^{-2}.

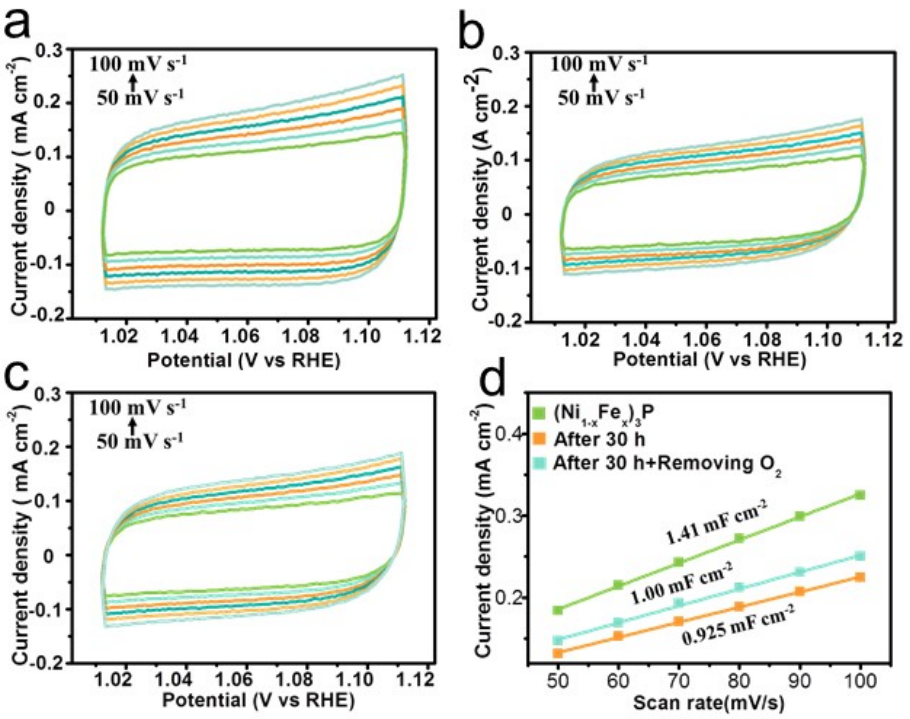

Figure S6. Measurements for electrochemical surface area (ECSA)**.** (a) CV curves of $(Ni_{1-x}Fe_x)_3P$, (b) CV curves of $(Ni_{1-x}Fe_x)_3P$ after 30 hours stability measurement, (c) CV curves of $(Ni_{1-x}Fe_x)_3P$ after 30 hours stability measurement and removing O_2 and (d) current differences plotted against scan rates.

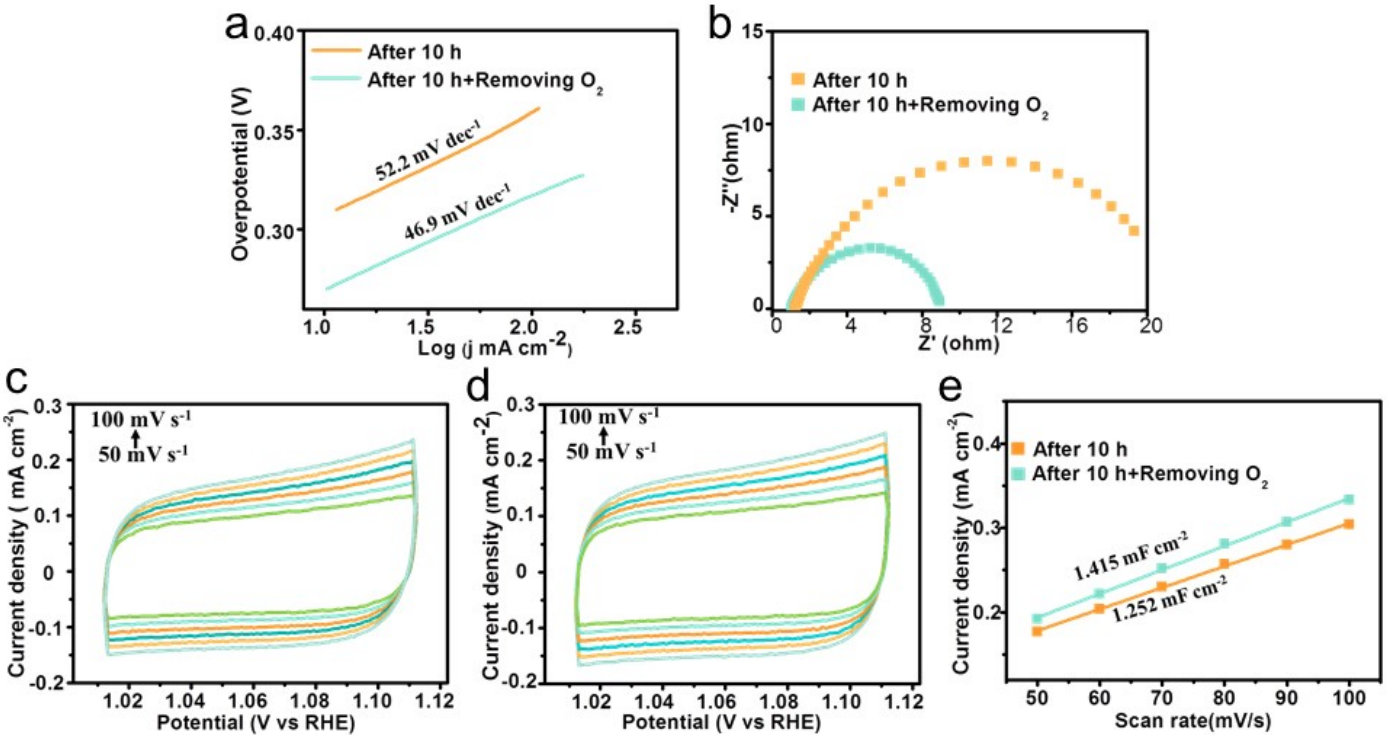

Figure S7. OER performance of $(Ni_{1-x}Fe_x)_3P$ after 10 hours stability measurement. (a) Tafel slopes before and after removing O_2. (b) EIS spectra before and after removing O_2 (c) CV curves for ECSA before removing O_2, (d) CV curves for ECSA after removing O_2 and (e) current differences plotted against scan rates.

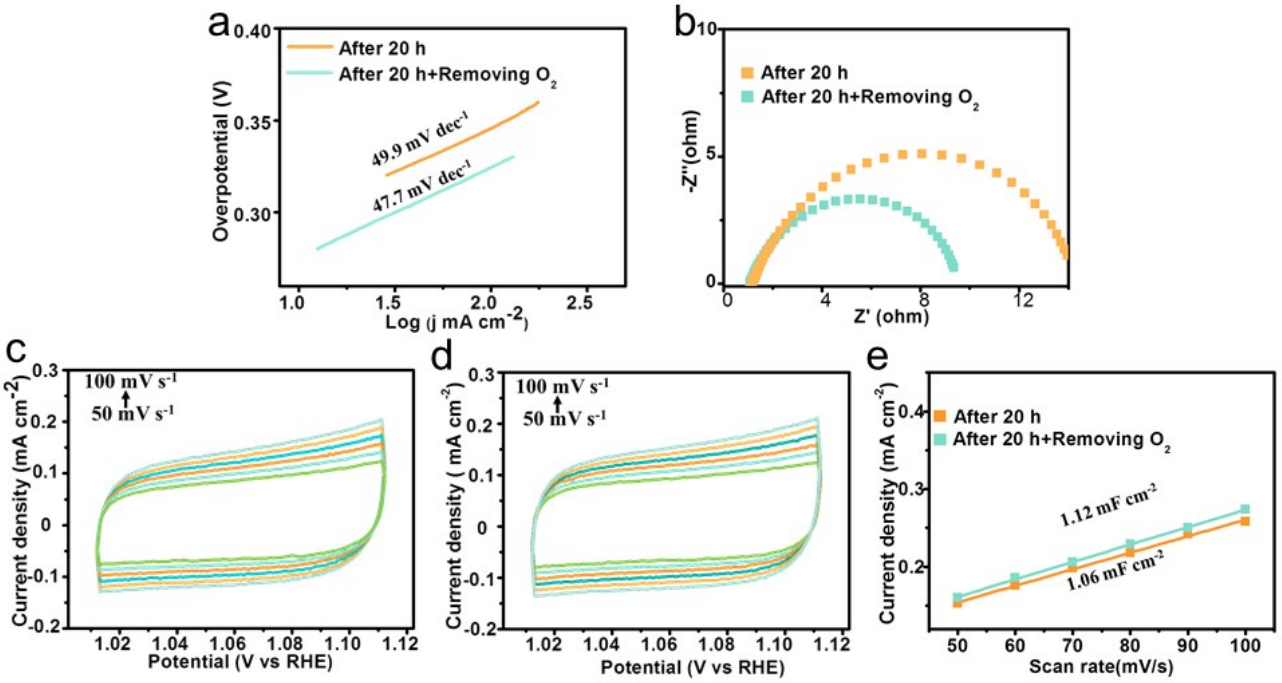

Figure S8. OER performance of $(Ni_{1-x}Fe_x)_3P$ after 20 hours stability measurement. (a) Tafel slopes before and after removing O_2. (b) EIS spectra before and after removing O_2 (c) CV curves for ECSA before removing O_2, (d) CV curves for ECSA after removing O_2 and (e) current differences plotted against scan rates.

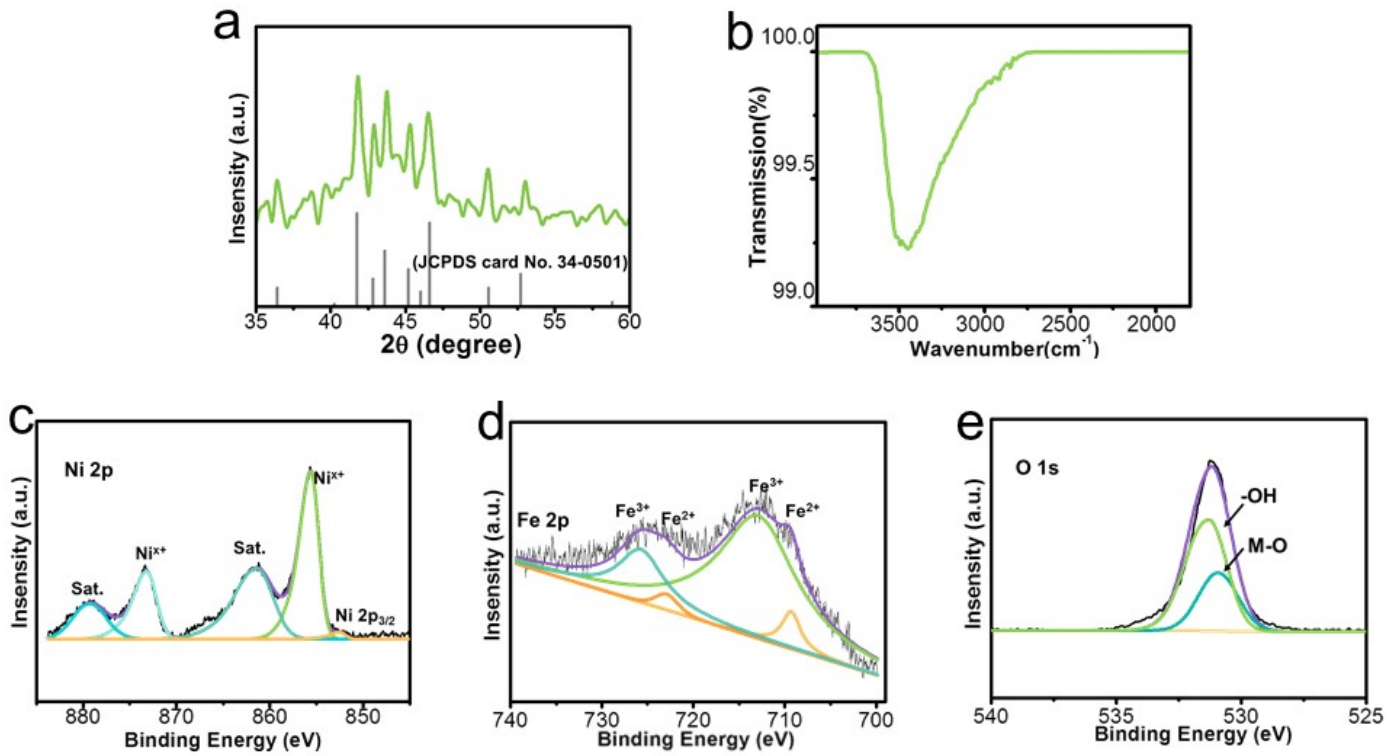

Figure S9. Characterizations of superareophobic heterostructure. (a) XRD pattern. (b) FTIR spectrum. (c) Ni 2p XPS s spectrum, (d) Fe 2p XPS spectrum and (e) O 1s XPS spectrum.

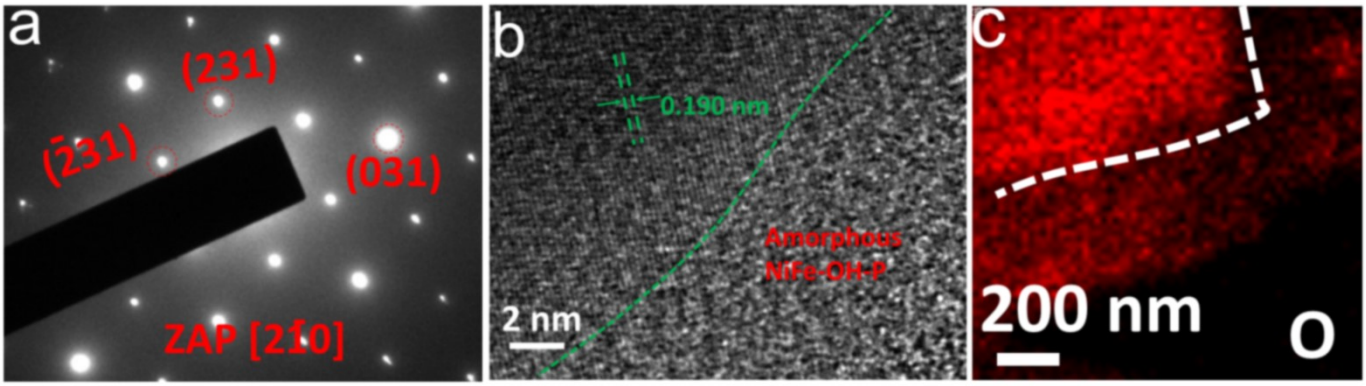

Figure S10. (a) SAED pattern, (b) HRTEM image and (c) EDS elemental mapping image of superareophobic heterostructure.

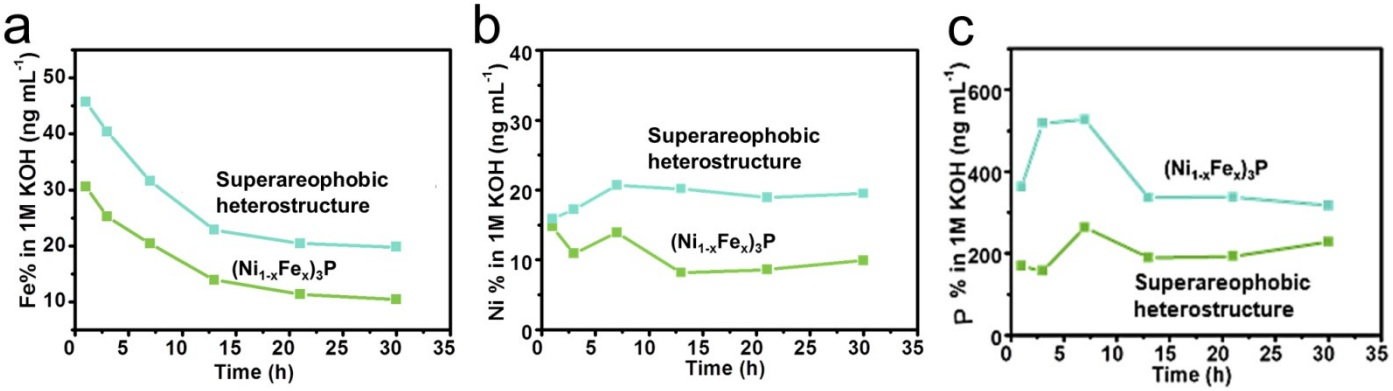

Figure S11. ICP-MS measurements for (a) Fe concentration, (b) Ni concentration and (c) P concentration in electrolyte during stability test.

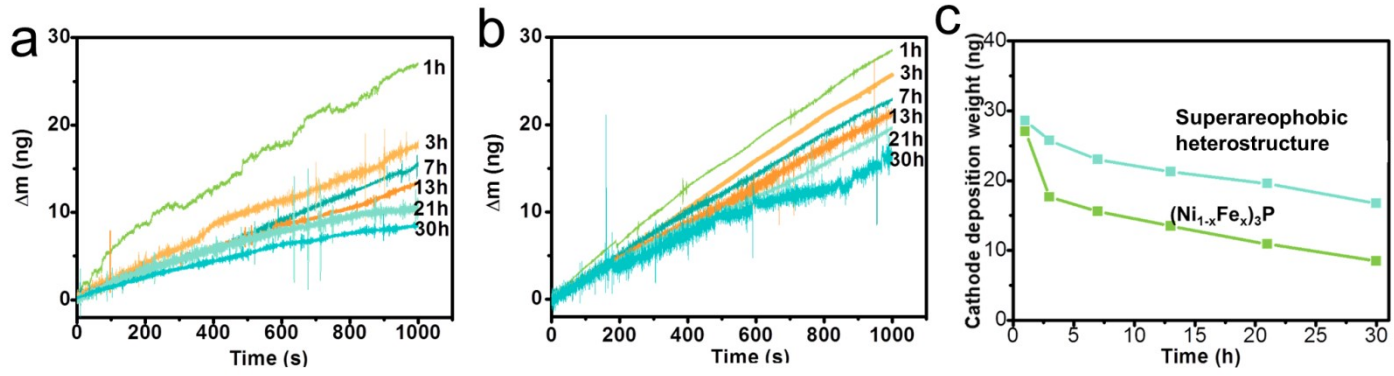

Figure S12. EQCM measurements for both Fe and Ni concentration in electrolyte during stability test for (a) $(Ni_{1-x}Fe_x)_3P$ and (b) superareophobic heterostructure. (c) The results of EQCM measurements.

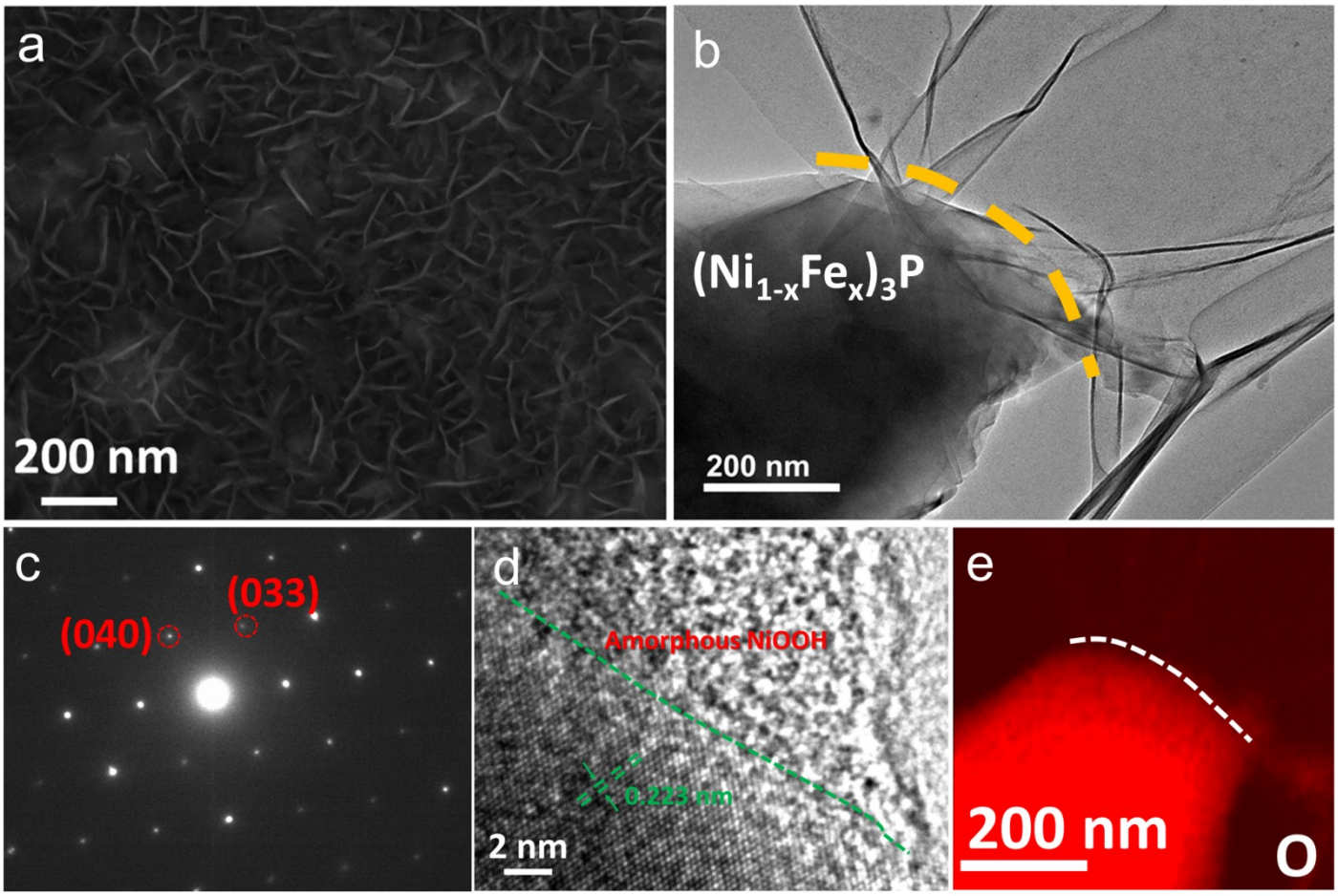

Figure S13. SEM and TEM Characterizations of superareophobic heterostructure after stability measurement. (a) SEM image, (b) TEM image, (c) SAED pattern, (d) HRTEM image and (e) EDS elemental mapping image of O.

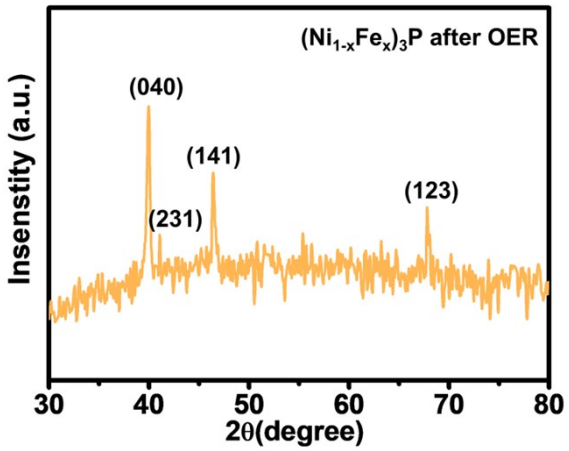

Figure S14. GIXRD patterns of the $(Ni_{1-x}Fe_x)_3P$ after 30 h stability measurement.

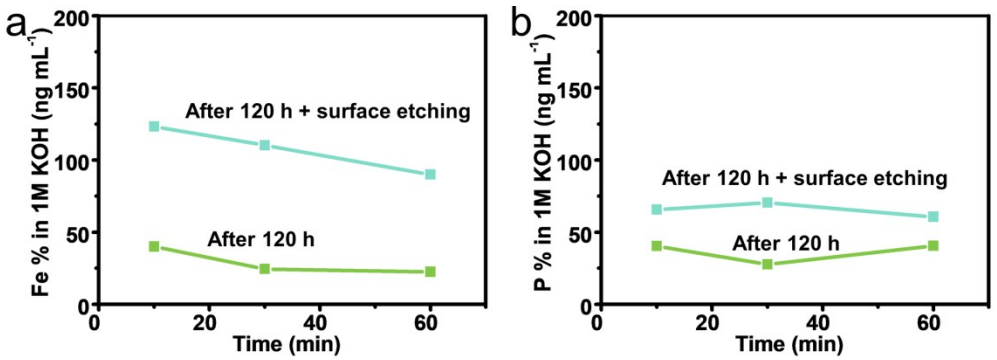

Figure S15 ICP-MS measurements for (a) Fe concentration and (b) P concentration in electrolyte during the OER test of superareophobic heterostructure at the current density of 100 mA cm^{-2}.

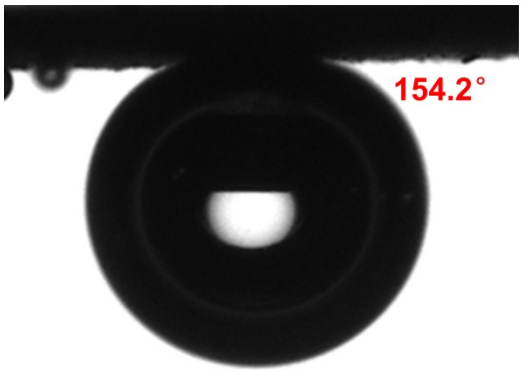

Figure S16 Bubble contact angle measurements of superareophobic heterostructure after 120 h stability measurement.

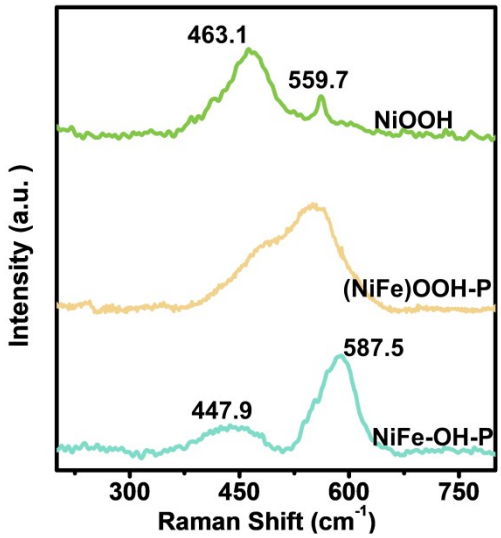

Figure S17 Raman spectra of NiOOH, (NiFe)OOH-P and NiFe-OH-P.

Table S1. Thermodynamic data used in the calculations of Gibbs free energy.

	E(eV)	ZPE - TS	G
H_2O	-14.218518	0.083711	-14.134807
H_2	-6.77	-0.047005	-6.817005
O_2	-	-	-9.71559
OH^-	-	-	-10.726305
$(Ni_{1-x}Fe_x)_3P$/NiOOH	-608.52164	0	-608.52164
$(Ni_{1-x}Fe_x)_3P$/NiOOH-OH*	-620.07073	0.315949	-619.75478
$(Ni_{1-x}Fe_x)_3P$/NiOOH-O*	-615.86816	0.0460	-615.82216
$(Ni_{1-x}Fe_x)_3P$/NiOOH-OOH*	-623.97726	0.37904	-623.59822
NiOOH	-387.89935	0	-387.89935
NiOOH-OH*	-398.61521	0.335117	-398.28009
NiOOH-O*	-393.10524	0.081	-393.02424
NiOOH-OOH*	-402.69087	0.260536	-402.43033
$(Ni_{1-x}Fe_x)_3P$-O/NiOOH	-655.2196	0	-655.2196
$(Ni_{1-x}Fe_x)_3P$-O/NiOOH-OH*	-665.15976	0.322908	-664.83685
$(Ni_{1-x}Fe_x)_3P$-O/NiOOH-O*	-659.84272	0.041465	-659.80126
$(Ni_{1-x}Fe_x)_3P$-O/NiOOH-OOH*	-669.87502	0.275137	-669.599883

Table S2. The results of EDS mapping

	$(Ni_{1-x}Fe_x)_3P$	$(Ni_{1-x}Fe_x)_3P$/NiFeOOH-P after 30 h	(NiFe)OOH-P after 10 h	(NiFe)OOH-P after 30 h
	Atomic percent (%)	Atomic percent (%)	Atomic percent (%)	Atomic percent (%)
P	25.15	24.76	12.18	3.55
Fe	8.59	6.14	10.64	1.46
Ni	66.26	69.10	77.18	94.99